The variations of stable carbon isotope ratio of land plant-derived *n*-alkanes in deep sea sediments from the Bering Sea and the North Pacific Ocean during the last 250,000 years

NALIN PRASANNA RATNAYAKE[1), 3)], NORIYUKI SUZUKI[1), *]
MAKOTO OKADA[2)], and MIYUKI TAKAGI [2)]

[1)] Division of Earth and Planetary Sciences, Graduate School of Science, Hokkaido University, N10 W8, Kita-Ku, Sapporo, 060-0810, Japan
[2)] Department of Environmental Science, Ibaraki University, 2-1-1, Bunkyo, Mito 310-8512, Japan
[3)] Present Address: Department of Earth Resources Engineering, Faculty of Engineering, Moratuwa University, Katubedda, Moratuwa, Sri Lanka

* Corresponding author:
NORIYUKI SUZUKI
Division of Earth and Planetary Sciences, Graduate School of Science, Hokkaido University, N10 W8, Kita-ku, Sapporo 060-0810, Japan
Tel: +81-11-706-2730, Fax: +81-11-746-0394
E-mail suzu@ep.sci.hokudai.ac.jp

Abstract

Two piston cores, one located far from the continents (The North Pacific Ocean: ES core), and another located comparatively closer to the continents (The Bering Sea: BOW-8a core) were investigated to reconstruct environmental changes on source land areas. The results show significant contribution of terrestrial organic matter to sediments in both cores. The $\delta^{13}C$ values of *n*-C_{27}, *n*-C_{29}, and *n*-C_{31} alkanes in sediments from the North Pacific ES core show significant glacial to interglacial variation whereas those from the Bering Sea core do not. Variations of $\delta^{13}C$ values of land plant *n*-alkanes are related to the environmental or vegetational changes in the source land areas. Environmental changes, especially, aridity, rainfall, and pCO_2 during glacial/interglacial transitional periods can affect vegetation, and therefore C_3/C_4 plant ratios, resulting in $\delta^{13}C$ changes in the preserved land plant biomarkers. Maximum values of $\delta^{13}C$ as well as maximum average chain length values of long chain *n*-alkanes in the ES core occur mostly at the interglacial to glacial transition zones reflecting a time lag related to incorporation of living organic matter into soil and transportation into ocean basins via wind and/or ability of C_4 plants to adapt for a longer period before being replaced by C_3 plants when subjected to gradual climatic changes. Irregular variations with no clear glacial to interglacial trends in the BOW-8a core may result from complex mixture of aerosols from westerly winds and riverine organic matter from the Bering Sea catchments. In addition, terrestrial organic matter entering the Bering Sea could originate from multiple pathways including eolian, riverine, and ice rafted debris, and possibly be disturbed by turbidity and other local currents which can induce re-suspension and re-sedimentation causing an obliterated time relation in the Bering Sea biomarker records.

Keywords: Bering Sea; Pacific Ocean; *n*-alkanes; stable carbon isotope; deep-sea sediments; higher plants; average chain length

1. Introduction

Time series sediment samples from marine cores are often utilized to reconstruct paleoclimatic and paleoceanographic environments. In addition to organic matter derived from marine organisms, ocean sediments also contain terrestrial organic matter. Long-chain *n*-alkanes and fatty acids are common biomarkers found in ocean sediments (Meyers, 1997; Hu et al., 2002; Pelejero, 2003; Ratnayake et al., 2005) and aerosols (Conte and Weber, 2002; Simoneit et al., 1977). These biomarkers are abundant components of land plant epicuticular waxes (Cranwell, 1973; Rieley et al., 1991), occurring as protective coatings on plant leaves. Wax particles are easily lost from the surfaces of leaves by wind ablation, and can become airborne (Conte and Weber, 2002). In addition, decomposing plant organic matter in soils can be airlifted during dust storms and carried by wind. Plant-wax lipids are therefore even found in dust above deep ocean areas, i.e., the North Pacific (Gagosian et al., 1981), the South Pacific (Gagosian et al.,1987), the eastern Atlantic (Simoneit, 1977), and western north Atlantic (Conte and Webber, 2002). The eolian fraction in the ocean basins depends mostly on the climate of the source area, and partially on the strength of winds, the distance from source area, and the number of transport episodes within the year.

Among various parameters for the reconstruction of environmental change on land, compound specific stable carbon isotope ratios ($\delta^{13}C$) are of great interest. Compound specific $\delta^{13}C$ values can refine the interpretation of bulk $\delta^{13}C$ data and further strengthen the reconstruction of paleoenvironmental changes (Bird et al., 1995; Huang et al., 1999). The $\delta^{13}C$ values of leaf wax biomarkers can be applied to evaluate relative contribution of C_3 versus C_4 plants. The C_4 plants are favoured in arid environments to adjust into water limitations resulting in less isotopic fractionation than the C_3 plants. Leaf waxes from C_4 plants usually have $\delta^{13}C$ values of about -23 ‰, whereas C_3 leaf waxes have $\delta^{13}C$ values of about -34 ‰

(Freeman and Colarusso, 2001). The $\delta^{13}C$ values of land plant waxes such as long chain *n*-alkanes in marine sediments have been used to determine vegetational contributions by C_3/C_4 plant type organic material to marine sediments (Bird et al., 1995; Kuypers et al., 1999; Huang et al., 2000; Hughen et al., 2004).

The present study focuses on the relationship between the variation of the land plant $\delta^{13}C$ values of *n*-C_{27}, *n*-C_{29}, and *n*-C_{31} alkanes and glacial/interglacial changes over the past 250,000 years. We obtained two piston cores from seamounts in the North Pacific Ocean and the Bering Sea. Organic matter from these sediments was analysed for the $\delta^{13}C$ of land plant *n*-alkanes. The results provide an insight into glacial/interglacial changes in the northeast Asia and Bering Sea catchment.

2. Study area and samples

Sampling of the sediment cores was carried out during Cruise KH99-3 of the R/V Hakuho Maru from June 25 to August 25, 1999. This cruise was organized by the Ocean Research Institute of the University of Tokyo to reconstruct the high–resolution glacial/interglacial paleoceanographic changes during the Late Quaternary in the Bering Sea and the North Pacific Ocean. Two piston cores were collected from representative sites (Fig. 1) in the Bering Sea (core BOW-8a from Bower Ridge) and the North Pacific Ocean (core ES from Emperor Seamount). The Bering Sea is a marginal sea linked to both the Pacific and the Arctic Oceans, and has a dynamic water circulation and convection pattern (Takahashi et al., 2000).

The cores collected were approximately 8.5 m long and consisted of clay, silty clay, and diatomaceous clay along with several intercalated volcanic ash bands. These cores were cut into several vertical sections and distributed among onboard scientists for multidisciplinary research including our organic geochemical studies. The samples were stored in stainless steel

cases at –20ºC and carried to the laboratory, where they were cut into 5 cm sections, freeze dried, ground, and used for organic matter extraction.

3. Experimental

3.1 Lipid Extraction

After the addition of $C_{24}D_{50}$ and $C_{30}D_{62}$ as internal standards (iSTD), approximately 5g of pulverized sample from each sediment section was subjected to ultrasonic lipid extraction by BIORUPTOR BD-1 (Cosmo Bio Co.) for 15 min with dichloromethane/methanol (9:1) mixed solvent. Sediments were extracted for three times (using total 100 ml of solvent). Solvent extracts were fractionated by silica gel (Wakogel Q-23) column chromatography (c.a. 10 cm x 1.6 cm ϕ) with *n*-hexane (25 ml) for saturated hydrocarbons. The saturated hydrocarbon fraction was analysed by Gas Chromatography (GC), Gas Chromatography–Mass Spectrometry (GC-MS), and Gas Chromatography–Combustion/Isotope Ratio Mass Spectrometry (GC-C/IRMS).

3.2 Instrumental

The saturated hydrocarbons were analysed using a Hewlett Packard HP6890/5973 GC-MS (splitless injection system) equipped with a fused silica column HP-5MS (30m × 0.25mm). The GC was programmed isothermally at 40ºC for 2 min., from 40ºC to 300ºC at 4ºC /min and held at 300ºC isothermally for 25 minutes. Concentrations of *n*-alkanes were determined based on their peak areas compared to those of deuterated internal standards.

The saturated hydrocarbons were also analysed using GC-C/IRMS, using a HP 6890 series GC (splitless injection system) equipped with fused silica capillary column DB-5 (30m× 0.25mm, J&W) coupled with a Finnigan MAT-252 Isotope Mass Spectrometer and a Finnigan MAT Interface GC-combustion III. The GC was programmed isothermally at 40ºC for 2.5 minutes, from 40ºC to 120ºC at 20ºC /min, from 120ºC to 300ºC at 4ºC /min. and held at 300ºC isothermally for 25 minutes. The $\delta^{13}C$ of *n*-alkanes were determined compared to iSTD, and are reported in per mill (‰) relative to the PDB standard. The error of the measurement calculated using iSTD is within ± 0.3 ‰.

3.3 Precision and accuracy of $\delta^{13}C$ measurements

Precision and accuracy are vital in measuring $\delta^{13}C$. We used the following precautionary procedure to increase the reproducibility of our $\delta^{13}C$ measurements. The standard deviation of the two iSTDs calculated using all the analysed samples (N=154, STDEV=0.3) was considered as the error range, and if the iSTD for a particular sample had a $\delta^{13}C$ value beyond ±0.3 ‰. of the mean iSTD values, such samples were reanalysed. Additionally, 28 samples from the ES core and 21 samples from the BOW-8a core randomly selected were replicated. The error range of these measurements was within ± 0.2 ‰. An external reference that contained *n*-C_{21}, *n*-C_{27}, *n*-C_{32} and *n*-C_{36} alkanes was measured after analysis of each ten samples to further enhance the reliability. The $\delta^{13}C$ values of these standards were determined using open inlet method (accuracy: ± 0.1 ‰).

3.4 Dating

The age models for Core BOW-8a and Core ES were established by Okada et al. (2005) by means of correlation between benthic foraminifera oxygen isotopes and the SPECMAP

stack (Imbrie et al., 1984, Martinson et al., 1987). Contrary to core BOW-8a, where abundance of foraminifera, *N. pachyderma (sinistral)*, allowed the establishment of a $\delta^{18}O$ of adequate resolution, in core ES, theses analyses could only be performed in discrete intervals. For this reason, this core was dated using another strategy (Katsuki et al., 2003), making use of the magnetic susceptibility data, which was tuned to the same measurements in a neighbour core (ODP Site 883) that had an already established age model (Keigwin, 1995). In Fig. 2, we have represented both magnetic susceptibility records, which exhibit a clear parallelism.

4. Results

According to the established age models, both BOW-8a and ES cores cover 250,000 years (Fig. 2), including almost nine glacial/interglacial periods (Martinson et al., 1987; Imbrie et al., 1992). The sediments are mostly of clay and silt, with intercalated diatomaceous and calcareous clays, along with several water-lain volcanic ash layers. The ES core had a total organic carbon (TOC) ranging from 0.25 to 0.9 % (average: 0.42 %) whereas the BOW-8a core had a TOC ranging from 0.3 % to 2.5 % and a higher average of 0.94 %. There was no significant glacial/interglacial variation with respect to the TOC change in either core.

Representative total ion chromatograms of *n*-alkanes obtained from GC-MS analysis of the ES and BOW-8a cores show similar distribution and abundance patterns (Fig. 3). They are characterized by uni-modal distributions with maxima at *n*-C_{27}, *n*-C_{29}, or *n*-C_{31}. Chain lengths are in the range from *n*-C_{17} to *n*-C_{35}, and the most prominent *n*-alkanes were *n*-C_{27}, *n*-$C_{29,}$ and *n*-C_{31}, whereas *n*-C_{17} and *n*-C_{18} alkanes occurred in low abundances. Normal alkanes having more than 23 carbons were generally abundant compared to those with fewer carbons. The carbon preference index (CPI) of the ES core (Table 1, and Fig. 4) ranges from 1.4 to 4.5 (average 3.1) whereas in BOW-8a (Table 2 and Fig. 5) it ranges from 1.8 to 7.6 (average 5.0). The higher to lower *n*-alkane ratio $\{H/L=(C_{25}+C_{27}+C_{29}+C_{31})/(C_{15}+C_{17}+C_{19})\}$ in the ES core

ranges from 1.0 to 26.6 (average 13.1) but in the BOW-8a core it varied from 3 to more than 100. Both CPI values and H/L ratios were greater throughout the BOW-8a core compared to ES core. However, these parameters do not vary in synchronous with glacial/interglacial changes. On the contrary, mass accumulation rates (MARs) of long chain *n*-alkanes (C_{27}+C_{29}+C_{31}) show significant glacial interglacial changes in both ES and BOW-8a cores. In ES core, MARs change from 0.07 to 1.1 $\mu gcm^{-2}kyr^{-1}$ and glacial stages generally show higher values, particularly during marine isotopic stage (MIS) 2 compared to interglacial periods (Ratnayake et. al., 2004). In BOW-8a core, MARs of long chain *n*-alkanes change from 0.35 to 2.1 $\mu gcm^{-2}kyr^{-1}$, with higher values during the glacial periods and lower values during the interglacial periods, similar to ES core. Average chain length (ACL) of long chain *n*-alkanes ranges from 29.3 to 28.4 (σ = 0.217) in ES core whereas in BOW-8a core it ranges from 29.2 to 28.6 (σ = 0.138). ACL shows a fairly good positive linear correlation with $\delta^{13}C$ values of C_{29} *n*-alkanes (R= 0.67) (Fig. 6), whereas in Bering core no correlation exists between these two parameters.

The compound specific $\delta^{13}C$ data obtained from isotopic monitoring gas chromatography show that the $\delta^{13}C$ of the ES core is in the –28 to –34 ‰ range (Table 1 and Fig. 4). Generally, during the glacial periods, the $\delta^{13}C$ values had an increasing trend, whereas during interglacial periods, $\delta^{13}C$ values had a decreasing trend, with an approximate variation of 1-3 ‰ during both stages (Fig. 4). Values become heavier at the end of the glacial periods and lighter at the end of the interglacial periods. The $\delta^{13}C$ values in core BOW-8a ranged from –29.5 to –34 ‰, but there was no significant glacial/interglacial change of $\delta^{13}C$ values of long chain *n*-alkanes throughout the Bering Sea core (Table 2 and Fig. 5).

5. Discussion

5.1 Source of long chain n-alkanes in deep-sea sediments

Lower abundances of *n*-C_{17} and *n*-C_{18} alkanes in the ES and BOW-8a core sediments, as shown in Fig. 3, indicate a low algal and bacterial organic matter contents (Giger et al., 1980) whereas higher abundances of *n*-C_{27}, *n*-C_{29}, and *n*-C_{31} alkanes indicate the dominant organic source of land plant epicuticular waxes (Cranwell, 1973; Rieley et al., 1991a). Higher CPI values, which denote the odd over even carbon predominance, of both cores (Figs. 4 and 5) are also compatible with abundant land-derived organic matter (Bray and Evans, 1961; Kolattukudy et al., 1976). Light $\delta^{13}C$ values in the range from –29 to –34 ‰ in our cores also confirm the terrestrial origin of the *n*-C_{27}, *n*-C_{29}, and *n*-C_{31} alkanes rather than marine origin (Meyers, 1997).

Terrestrial organic matter supplied to the open North Pacific Ocean is likely to be derived mostly from mid latitudes, transported by the prevalent westerly winds. Rea (1990) showed that the eolian contribution to the North Pacific Ocean is quite significant. Terrestrial organic matter derived from the high latitude Bering Sea catchment area and carried by river and oceanic currents to the ES core site is probably less significant, as this area is located far from land. On the contrary, the BOW-8a core contains terrestrial organic matter predominantly from the high latitude Bering Sea catchments carried by river currents, with minor contribution from westerly winds.

5.2 Variations of $\delta^{13}C$ and ACL of long chain n-alkanes during the last 250,000 years

The ES core shows distinctive correlation of $\delta^{13}C$ values (Fig. 4) of higher plant *n*-alkanes (C_{27}, C_{29} and C_{31}) with respect to glacial/interglacial changes. The $\delta^{13}C$ maxima occur mostly at the beginning of the interglacial periods. In general terms, the observed trends tend to decrease during interglacial periods (-1 to -4 ‰) and to increase during glacial periods (1 to 4 ‰) (Fig. 4). Similar trends can also be seen with respect to ACL indexes, which exhibit

distinct higher values at the beginning of the interglacial periods. Recent studies show that ACL varies with arid/humid vegetational sources where the relative proportion of C_3 to C_4 plant changes (Huang et al., 2000; Schefuß et al., 2003; Hughen et al., 2004; Calvo et al., 2004). For example, aeolian dust samples collected in transects along the West African coast show a change in the chain length distributions of *n*-alkanes as a response to aridity in the source regions (Huang et al., 2000). In addition, leaf wax biomarkers preserved in Cariaco basin sediments reveal chain length variability that correlates strongly with *n*-alkane $\delta^{13}C$ changes (Hughen et al., 2004). Similarly, long chain *n*-alkanes from southern paleosols and Bengal Fan sediments show a strong correlation between chain length variability and Miocene C_4 plant expansion (Freeman and Colarusso, 2001). On the other hand, Calvo et al. (2004) also found a climate dependence of ACL values, with longer chains occurring during glacial period. The present study also shows a climate dependence of ACL and a significant correlation between $\delta^{13}C$ of long chain *n*-alkanes and ACL (Fig. 6). This correspondence let us suggest that our observed time series changes in the ES core can be related to aridity changes in the source area that have resulted in changes in the relative abundance of C_3 versus C_4 plants.

According to Wang et al. (1999), two extremes of East Asian monsoon circulation alternate with the glacial to interglacial cycles during the Late Pleistocene. A strongly intensified winter-monsoon and weakened summer monsoon during glacial period reduced monsoonal precipitation during summer. In contrast, strengthened summer-monsoon circulation and weak winter-monsoon winds led to extreme continental wetness. Our observed $\delta^{13}C$ changes in the North Pacific Ocean core are probably driven by aridity changes that, on the other hand, are probably coupled to East Asian monsoonal changes in mid latitudinal land areas.

5.3 Changes of vegetation on land during the glacial and interglacial periods

Generally, a decreasing partial pressure of CO_2 and increasing aridness during glacial periods result in an increase of C_4 photosynthetic plants, which have much higher $\delta^{13}C$ values than C_3 photosynthetic plants (Ehleringer et al., 1997; Huang et al., 1999). Therefore, the gradual increase in $\delta^{13}C$ during glacial periods may indicate gradual increase of C_4 plants in the source area, whereas in interglacial periods the gradual decrease in $\delta^{13}C$ may indicate relative decrease of C_4 plants.

Change of C_3 plant types may also be able to explain observed time series changes in the ES core, since the $\delta^{13}C$ variation observed was small being less than 4 ‰. Pollen studies from Chinese loess beds show Northeast Asian vegetation has changed from forest to grasslands with interglacial to glacial transition in the last six oxygen stages (Feng et al., 1998). However, pollen analysis does not distinguish between C_4 and C_3 grass plants. According to present understanding of stable carbon isotope ratios, it is difficult to conclude that C_3 grass species have long chain *n*-alkane with higher $\delta^{13}C$ than do forest species. Lake core sediments collected from an old sedimentary basin near Bogotá, Colombia showed 1 to 2 ‰ lighter $\delta^{13}C$ values when the grass pollen percentage compared to the forest plants is low, and heavier $\delta^{13}C$ values about 1-2 ‰ when the grass pollen percentage is high (Boom et al., 2002). These authors concluded that heavier isotopic values, coinciding with glacial periods, are due to the increase of C_4 plants without considering the possibility of changes in C_3 plant types. Using soil carbonate, Han et al. (1997) demonstrated increase of C_4 plants during glacial periods in Northeast Asia. The variation of $\delta^{13}C$ of higher plant *n*-alkanes in the present study repeated systematically over the last nine oxygen isotopic stages. The increasing trends of $\delta^{13}C$ values with interglacial to glacial transition are probably due to gradual expansion of C_4 plants in the source area.

Variations of $\delta^{13}C$ and ACL during the glacial and interglacial periods in the present paper suggest that C_4 plants start to spread with the beginning of glacial periods and peak at the beginning of the interglacial periods. Subsequently, C_4 plants start to diminish gradually through the end of the interglacial stage. Therefore, we suppose there is a time lag between formation of C_4 plants in the source area and deposition in the North Pacific Ocean basin.

5.4 Transportation and deposition of long chain n-alkanes in the deep-sea basin

Time lag between higher plant formation on land and deposition in the deep-sea basin might be related to incorporation of organic matter into the soil and subsequent transportation. According to Takahashi et al. (2000) and Rea (1990), terrestrial organic matter is mainly derived from decomposed higher plants in soils, which can be airlifted during dust storms and carried by wind from mid latitudes to the Pacific Ocean. In this case, direct contribution from contemporary leaf waxes by wind ablation is minimal. MARs of long chain *n*-alkanes in this study (Fig. 4) also support that organic matter to the North Pacific Ocean is mainly carried with soil particles. Increase of MARs of long-chain *n*-alkanes in glacial periods recorded in ES core can be explained by higher dust input during glacial periods due to aridity in the source area coupled by stronger global atmospheric circulation. Organic matter attached to such dust particles was probably the reason for the increase of MARs of long chain *n*-alkanes. C_4 plant input from North West Africa into North East Atlantic surface sediments reveals large input of ancient C_4 plant waxes into present day sediments derived from 8,500- 3000 years B. P. compared to present day (Huang et al., 2000). On the other hand, time lag in the North Pacific Ocean core is also due to time lag involved in vegetational response. This may indicate the ability of C_4 plants to adapt for a longer period before being replaced by C_3 plants when faced with gradual climatic changes.

Irregular $\delta^{13}C$ variation of long chain *n*-alkanes in the BOW-8a core (Fig. 5) could be due to insignificant mid latitude aerosol content, compared to river-supplied organic matter from the Bering Sea catchment area, where C_4 plants may be less widespread due to cold arid climate during the glacial periods. The $\delta^{13}C$ time series change of the ES core may represent vegetational changes in mid latitudes, whereas that of the BOW-8a core represent vegetational changes in high latitude Bering Sea catchments. However, it is also important to consider that the terrestrial organic matter coming to the Bering Sea via river waters is a mixture of plant litter and soil matter, which could be both modern and paleosol in origin. Also, turbidity currents and other local currents could result in re-suspension of organic matter and re-sedimentation, causing deposition of organic matter with a wide range of geologic ages. Studies of $\delta^{13}C$ of land plant *n*-alkanes in the Japan Sea (Yamada and Ishiwatari, 1999) and the China Sea (Hu et al., 2002) do not show variations similar to those recorded in the ES core. These areas received considerable terrestrial organic matter from river water, and possibly also reworked organic matter from turbidity and other currents, obliterating the isotopic signal. The numerous river systems in the Japan Sea favour fluvial transport of plant material from the riverside vegetation. This process probably account for more negative $\delta^{13}C$ values and thus for more C_3 plants (Huang, et al., 2000). The present study revealed significant glacial-interglacial changes of land plant $\delta^{13}C$ values and ACL recorded in deep-sea sediments from the North Pacific Ocean. These variations can be explained by changes of relative abundance of C_3/C_4 plants responding to changes of aridity in the North East Asia.

6. Conclusion

The $\delta^{13}C$ values of *n*-C_{27}, *n*-C_{29}, and *n*-C_{31} alkanes in core sediments from the North Pacific ES core show significant glacial to interglacial variation, whereas those from the Bearing Sea BOW-8a core do not. The ES core received terrestrial organic matter transported

by winds mainly from the mid latitudes, whereas BOW-8a received terrestrial organic matter from the high latitude Bering Sea catchment. The ES core received terrestrial materials mainly by wind, whereas that in the BOW-8a core had multiple provenances including eolian, riverine, and other transportation pathways. Original environmental fingerprint were well preserved in the ES core, while those in BOW-8a were disturbed by turbidity currents and other local currents, which could induce re-suspension and re-sedimentation of older organic matter at that site.

The observed glacial/interglacial $\delta^{13}C$ (land plant *n*-alkanes) shifts in ES core can be explained by changes in the relative abundances of C_3 to C_4 plants or plant species changes in the source land area. These changes could be driven by East Asian monsoonal cycles along with aridity changes in mid latitudinal land areas. Peaking of $\delta^{13}C$ values at the beginning of the interglacial periods may indicate a time lag between vegetational changes in the source area, and/or deposition of organic matter in the ocean basin and/or ability of C_4 plant to adapt to climate change.

Variations in $\delta^{13}C$ of land plant alkanes in BOW core, however, probably reflect a combination of origins that prevent the extraction of conclusive paleoclimatic information. In the studied area, marine sediment cores collected from remote ocean areas are easier to interpret, particularly when considering that terrestrial materials there are mainly transported by wind as a single mechanism.

Acknowledgment

We thank Prof. K. Takahashi for arranging Cruise KH99-3 of the R/V Hakuho Maru, Prof. M. Minagawa for $\delta^{13}C$ measurement of reference standards, Dr. K. Sawada for his help and useful comments, and the Japanese Ministry of Education, Culture, Sports, Science and Technology, for a 21st Century Center of Excellence (COE) grant in the "Neo-Science of

Natural History" Program (Leader: Hisatake Okada) at Hokkaido University. Comments by Dr. C. Pelejero, Dr. T. Horscroft, and an anonymous reviewer substantially improved the manuscript.

References

Bird, M I., Summons, R. E., Gagan, M. K., Roksandic, Z., Dowling, L., Head, J., Fifield, L. K., Cresswell, R. G. and Johnson, D. P., 1995. Terrestrial vegetation change inferred from *n*-alkane $\delta^{13}C$ analysis in the marine environment. Geochimica et Cosmochimica Acta 59: 2853-2857.

Bray, E. E. and Evans, E. D., 1961. Distribution of *n*-paraffins as a clue to the recognition of source beds. Geochimica et Cosmochimica Acta. 22: 2-9.

Boom, A., Marchant, R., Hooghiemstra, H. and Sinninghe Damste J. S., 2002. CO_2 and temperature-controlled altitudinal shifts of C_4 and C_3 dominated grasslands allow reconstruction of palaeoatmospheric pCO_2. Palaeogeography, Palaeoclimatology, Palaeoecology 177: 151-168.

Calvo, E., Pelejero, C., Logan, G. A. and Deckker, P. De, 2004. Dust-induced changes in phytoplankton composition in the Tasman Sea during the last four glacial cycles. Paleoceanography 19: PA2020, doi:10.1029/2003PA000992.

Conte, M. H. and Weber, C. J., 2002. Plant biomarkers in aerosols record isotopic discrimination of terrestrial photosynthesis. Nature 417: 639-641.

Cranwell, P. A., 1973. Chain-length distribution of *n*-alkanes from lake sediments in relation to post-glacial environmental change. Freshwater Biology 3: 259-265.

Ehleringer, J. R., Cerling, T. E. and Helliker, B. R., 1997. C_4 photosynthesis, atmospheric CO_2 and climate. Oecologia 112: 285-299.

Feng, Z. D., Chen, F. H., Tang, L. Y. and Kang, J. C., 1998. East Asian monsoon climate and Gobi dynamics in marine isotope stages 4 and 3. Catena 33: 29-46.

Freeman, K. H. and Colarusso, L. A., 2001. Molecular and isotopic records of C_4 grassland expansion in the late Miocene. Geochimica et Cosmochimica Acta 65: 1439-1454.

Giger, W., Schaffner, C. and Wakeham, S. G., 1980. Aliphatic and olefinic hydrocarbons in recent sediments of Greifensee, Switzerland. Geochimica et Cosmochimica Acta 44: 119-129.

Gagosian, R. B., Peltzer, E. T. and Merrill, J. T., 1987. Long-range transport of terrestrially derived lipids in aerosols from the South Pacific. Nature 325: 800–803.

Gagosian, R. B., Peltzer, E. T. and Zafiriou, O. C., 1981. Atmospheric transport of continentally derived lipids to the tropical North Pacific. Nature 291: 312–314.

Han, J., Fyfe, W. S. and Longstaffe, F. J., 1997. Climate implications of S5 palesol complex on the southernmost Chinese loess plateau. Quaternary Research 50**:** 21-33.

Hu, J., Peng, P., Jia, G., Fang, D., Zhang, G., Fu, J. and Wang, P., 2002. Biological markers and their carbon isotopes as an approach to the paleoenvironmental reconstruction of Nansha area, South China Sea, during the last 30 ka. Organic Geochemistry 33: 1197-1204.

Huang, Y., Dupont, L., Sarnthein, M., Hayes, J. M. and Eglinton, G., 2000. Mapping of C_4 plant input from North West Africa into North East Atlantic sediments. Geochimica et Cosmochimica Acta 64: 20, 3505-3513.

Huang, Y., Street-Perrott, F. A., Perrott, R. A., Metzger, P. and Eglinton, G., 1999. Glacial-interglacial environmental changes inferred from molecular and compound-specific $\delta^{13}C$ analyses of sediments from Sacred Lake, Mt. Kenya. Geochimica et Cosmochimica Acta 63: 9, 1383-1404.

Hughen, K. A., Eglinton, T. I., Xu, L. and Makou, M. 2004. Abrupt tropical vegetation response to rapid climate changes. Science 304: 1955-1959.

Imbrie, J., Hays, J. D., Martinson, D. G., McIntyre, A., Mix, A. C., Morley, J. J., Pisias, N. G., Prell, W. L. and Shackleton, N. J., 1984. The orbital theory of Pleistocene

climate: support from a revised chronology of the marine $\delta^{18}O$ record. Berger, A. L. et al. (Eds.), Milankovitch and Climate, Part 1. D. Reidel. 269-305.

Imbrie, J., Boyle, E. A., Clemens, S. C., Duffy, A., Howard, W. R., Kukla, G., Kutzbach, J., Martinson, D. G., McIntyre, A., Mix, A. C., Molfino, B., Morley, J. J., Peterson, L. C., Pisias, N. G., Prell, W.L., Raymo, M. E., Shackleton, N. J. and Toggweiler, J. R., 1992. On the structure and origin of major glaciation cycles. 1. Linear responses to Milankovitch forcing, Paleoceanography, 7: 701-738.

Katsuki, K., Takahashi, K. and Okada, M., 2003. Diatom assemblage and productivity changes during the last 340,000 years in the subarctic Pacific. *Journal of Oceanography* 59: 695-707.

Keigwin, L. D., 1995. Stable isotope stratigraphy and chronology of the upper Quaternary section at Site 883. In: D. K. Rea, I. A. Basov, D. W. Scholl, and J. F. Allan (Editors), Proc. ODP, Sci. Results. College Station, TX (Ocean Drilling Program), 145, pp. 257-264.

Kolattukudy, P. E., Croteau, R. and Buckner, J. S., 1976. Biochemistry of plant waxes. In: P.E. Kolattukudy (Editor), Chemistry and Biochemistry of Natural Waxes. Elsevier, Amsterdam, pp. 289-347.

Kuypers, M. M. M., Pancost, R. D. and Sinninghe Damste, J. S., 1999. A large and abrupt fall in atmospheric CO_2 concentration during Cretaceous times. Nature 399: 342-345.

Martinson, D. G., Pisias, G. P., Hays, J. D., Imbrie, J., Moore, T. C., JR. and Shackleton, N. J., 1987. Age dating and the orbital theory of the ice ages: Development of a high-resolution 0 to 300,000-year chronostratigraphy. Quaternary Research 27:1-29.

Meyers, P. A., 1997. Organic geochemical proxies of paleoceanographic, paleolimnologic, and paleoclimatic processes. Organic Geochemistry 27: No. 5/6, 213-250.

Okada, M., Takagi, M. and Takahashi, K., 2005. Chronostratigraphy of sediment cores from the Bering Sea and the subarctic Pacific based on paleomagnetic and oxygen isotopic analyses. Submitted to Deep Sea Research II.

Pelejero, C., 2003. Terrigenous n-alkane input in the South China Sea: high-resolution records and surface sediments. Chemical Geology 200: 89-103.

Ratnayake, N. P., Suzuki, N., Matsubara, M. and Okada, M., 2004. Variation of mass accumulation rates of long chain *n*-alkanes in the Northern North Pacific During the last 350 kyrs. In: S. F. Mawatari, and H. Okada (Editors), Neo-Science of Natural History: Integration of Geosciences and Biodiversity Studies. (Proceedings of international symposium on "Dawn of a new natural history-integration of geosciences and biodiversity studies."), Sapporo, Japan, pp. 143-146.

Ratnayake, N. P., Suzuki, N. and Matsubara, M., 2005. Sources of long chain fatty acids in deep sea sediments from the Bering Sea and the North Pacific Ocean. Organic Geochemistry 36: 531-541.

Rea, D. K., 1990. Aspects of atmospheric circulation: the late Pleistocene (0–950,000 yr) record of eolian deposition in the Pacific Ocean. Palaeogeography, Palaeoclimatology, Palaeoecology 78: Issues 3-4, 217-227.

Rieley, G., Collier, R. J., Jones, D. M. and Eglinton, G., 1991. The biogeochemistry of Ellesmere Lake, U.K, I: Source correlation of leaf wax inputs to the sedimentary record. Organic Geochemistry 17: 901-912.

Schefuß, E., Ratmeyer, V., Stuut, J. W., Jansen J. H. F. and Sinninghe Damsté, J. S., 2003. Carbon isotope analyses of *n*-alkanes in dust from the lower atmosphere over the central eastern Atlantic. Geochimica et Cosmochimica Acta 67: 1757-1767.

Simoneit, B. R. T., Chester, R. and Eglinton, G., 1977. Biogenic lipids in particulates from the lower atmosphere over the eastern Atlantic. Nature 267: 682–685.

Takahashi, K., Fujitani, N., Yamada, M. and Maita, Y., 2000. Long-term biogenic particle fluxes in the Bering Sea and the central subarctic Pacific Ocean 1990-1995. Deep-Sea Research I, 47: 1723-1759.

Wang, L., Sarnthein, M., Erlenkeuser, H., Grimalt, J., Grootes, P., Heilig, S., Ivanova, E., Kienast, M., Pelegero, C. and Pflaumann, U., 1999. East Asian monsoon climate during the Late Pleistocene: high-resolution sediment records from the South China Sea. Marine Geology 156: 245-284.

Yamada, K. and Ishiwatari, R., 1999. Carbon isotopic compositions of long-chain *n*-alkanes in the Japan Sea sediments: implications for paleoenvironmental changes over the past 85 kyr. Organic Geochemistry 30: 367-377.

Table 1. Time series changes of CPI, ACL, and $\delta^{13}C$ values of long chain *n*-alkanes (C_{27},C_{29}, and C_{31}) from ES core, the North Pacific Ocean.

ES core											
Age	CPI	ACL	$\delta^{13}C$ ‰			Age	CPI	ACL	$\delta^{13}C$ ‰		
yr×1000			C_{27}	C_{29}	C_{31}	yr×1000			C_{27}	C_{29}	C_{31}
1.7	2.64	28.9	***-30.0***	***-31.0***	***-31.9***	147.4	2.66				
8.7	3.35					154.3	1.52				
10.1	2.73	28.8	***-29.5***	***-30.5***	***-31.1***	159.5	3.07	28.6	-30.3	-30.8	-31.2
11.4	3.23	28.7	-29.5	-31.3	-31.5	164.7	2.67	29.0	-29.6	-30.6	-31.3
12.7	2.29					169.3	3.74				
14.0	2.44	28.9	**-29.7**	**-31.7**	**-32.3**	171.8	2.30				
15.3	3.16	28.6	-30.3	-31.3	-32.3	173.9	2.92	28.6	***-29.8***	***-30.1***	***-31.4***
16.5	2.99	28.5	*-30.4*	*-32.4*	*-32.4*	175.9	3.60	28.8	-30.1	-30.9	-32.2
18.9	3.09	28.5	***-30.4***	***-31.2***	***-32.6***	182.0	3.84	28.7	-30.8	-31.0	-31.6
23.9	2.96	28.6	**-30.9**	**-32.5**	**-33.4**	188.5	3.60	28.7	-30.8	-31.9	-31.7
28.4	3.23	28.4	-31.0	-32.6	-33.5	195.0	4.13	28.5	**-31.3**	**-31.4**	**-31.9**
31.7	2.76	28.4	-31.2	-33.4	-33.8	201.5	3.06				
35.0	3.33	28.6	-30.9	-33.5	-32.2	208.2	3.35				
38.3	3.24	28.4	***-30.8***	***-33.5***	***-33.7***	215.8	2.36	28.7	-30.6	-30.7	-31.4
41.7	3.08	28.9	-30.2	-32.6	-32.5	221.8	3.61	28.5	**-31.3**	**-31.4**	**-32.4**
44.2	3.13	28.8	-30.1	-32.7	-32.7	224.5	3.87	28.8	-31.0	-31.9	-31.6
46.2	3.24	28.8	**-30.1**	**-32.6**	**-32.0**	227.0	3.56	28.8	-30.8	-31.2	-32.4
47.2	3.80	28.8	-30.0	-32.1	-31.3	229.4	3.41	28.7	**-30.3**	**-31.0**	**-31.8**
49.4	3.50	28.9	***-30.1***	***-31.6***	***-31.9***	231.7	3.12	29.1	-29.6	-30.2	-29.7
51.5	3.95	28.8	-29.9	-31.1	-32.6	239.3	2.67	29.0	***-29.2***	***-30.3***	***-30.6***
53.7	4.18	28.9	***-30.0***	***-31.5***	***-32.0***	247.4	3.03	29.0	-29.8	-30.6	-30.3
55.9	3.27					255.5	3.22		-30.2	-30.2	
58.1	3.54	28.8	-30.7	-31.5	-32.8	259.2	3.70	29.2	-30.1	-30.4	-30.4
60.2	3.23	28.5	-30.2	-31.7	-32.8	262.7	1.83	29.1	**-30.0**	**-30.5**	**-30.8**
62.5	3.35	28.5	-31.1	-31.5	-33.2	265.9	2.96	29.0	-30.3	-30.8	-30.7
66.0	3.60	28.5	***-31.7***	***-32.0***	***-33.0***	269.6	2.96	28.7	-31.0	-30.8	-31.2
69.4	3.43	28.7	-30.7	-31.3	-31.8	274.3	3.55	28.8	**-30.9**	**-31.0**	**-31.3**
71.5	3.82	28.6	-32.0	-32.3	-32.5	279.0	3.25	28.9	-30.8	-30.7	-32.5
74.9	3.59	28.9	***-31.1***	***-31.1***	***-31.6***	283.7	3.57	28.8	-30.6	-31.2	-32.0
78.3	3.48	28.8	-30.3	-31.1	-32.5	288.4	3.46	28.8	**-30.0**	**-30.1**	**-31.3**
81.8	2.44	28.9	**-29.0**	**-30.4**	**-30.4**	293.1	3.30	28.8	-30.5	-30.8	-31.5
85.5	1.93	29.1	-28.7	-30.2	-30.3	298.7	3.16		-30.4	-30.9	
89.3	2.70	28.9	-29.6	-30.6	-30.5	304.7	3.51	28.7	**-31.6**	**-31.7**	**-32.6**
93.0	1.99	28.8	***-28.2***	***-29.7***	***-30.5***	309.3	3.07				
96.7	2.77	28.8	-29.0	-30.2	-30.7	312.6	4.50	28.9	***-29.9***	***-30.7***	***-30.7***
100.5	2.52	28.8	-28.8	-30.6		316.0	3.83	28.9	-30.5	-30.6	-30.3
104.2	2.22	29.2	-28.6	-30.0	-29.4	319.3	3.67	29.1	-29.8	-29.9	-30.3
107.4						322.6	2.65	29.2	**-30.8**	**-30.7**	**-30.1**
112.0	3.14	28.9	-29.3	-30.1	-29.7	326.6	1.63				
116.5	3.75	29.2	***-28.8***	***-30.2***	***-29.4***	332.4	2.89	29.1	-29.7	-30.4	-30.2
121.0	3.27	29.3	-29.9	-29.7	-29.6	338.1	2.95	29.2	-29.0	-30.0	-30.3
126.7	2.34	29.1	**-29.6**	**-30.3**	**-30.9**	343.8	2.18				
133.6	2.61	29.2	-29.7	-30.1	-30.0	348.2	2.15	29.2	**-30.5**	**-30.4**	**-31.0**
140.5	2.75	28.7	**-29.4**	**-30.2**	**-31.0**						

Bold $\delta^{13}C$ values are duplicates while bold-italic values are triplicates.

Table 2. Time series changes of CPI, ACL, and $\delta^{13}C$ values of long chain *n*-alkanes (C_{27}, C_{29}, and C_{31}) from BOW-8a core, the Bering Sea.

BOW-8a core												
Age	CPI	ACL	$\delta^{13}C$ ‰			Age	CPI	ACL	$\delta^{13}C$ ‰			
yr×1000			C_{27}	C_{29}	C_{31}	yr×1000			C_{27}	C_{29}	C_{31}	
3.0	3.24	29.1	***-29.3***	***-30.0***	***-29.8***	151.2	5.60	29.0	-29.9	-30.7	-31.9	
6.1	1.80	29.1	-32.3	-31.8	-31.5	155.1	5.42	29.0	-30.2	-30.9	-31.8	
8.2	2.62	29.0	**-29.7**	**-29.6**	**-31.9**	158.0	5.04	28.9	-30.9	-31.1	-32.2	
10.3	3.82	28.9	-32.1	-30.9	-31.8	160.3	5.19	28.9	-30.0	-30.7	-31.9	
12.3	4.49	28.9	***-29.9***	***-31.0***	***-31.6***	162.5	6.99	28.6	-29.8	-30.6	-31.1	
14.4	4.64	28.9	-29.8	-31.1	-31.4	164.8	5.92	28.7	-29.8	-30.6	-31.6	
16.4	4.61	28.9	-30.1	-31.0	-32.1	167.1	6.21	28.8	***-28.9***	***-29.9***	***-31.0***	
22.4	4.52	28.6	-30.1	-30.7	-31.8	169.4	6.35	28.9	-29.5	-30.8	-30.6	
29.7	4.08	28.8	***-29.9***	***-30.7***	***-31.6***	171.7	5.75	28.7	-29.9	-30.4	-31.0	
35.1	5.01	28.7	-30.0	-31.0	-31.8	173.8	7.63	28.7	-29.8	-30.6	-31.1	
40.5	5.21	28.7	**-29.8**	**-31.3**	**-32.0**	175.3	7.12	28.8	-29.7	-31.3	-32.2	
43.6	5.68	28.8	-30.4	-30.8	-31.8	175.6	6.58	29.0	-29.9	-31.4	-32.4	
45.3	5.34	28.8	**-30.5**	**-31.4**	**-32.0**	176.0	5.73	28.9	-30.7	-32.7	-32.9	
47.0	5.37	28.8	-29.5	-30.1	-31.4	176.3	6.17	28.9	**-30.3**	**-31.7**	**-32.3**	
48.8	5.25	28.8	***-29.9***	***-30.2***	***-31.4***	176.7	6.22	29.0	-30.5	-33.1	-31.3	
50.5	5.25	28.8	-29.5	-30.7	-31.7	177.0	6.07	28.7	-29.8	-32.6	-32.0	
52.2	5.33	29.0	-30.4	-31.1	-31.8	177.4	5.52	28.7	-29.7	-31.0	-32.6	
53.9	5.32	29.0	-30.5	-30.4	-31.6	177.8	5.05	28.6	-29.7	-30.3	-30.7	
55.5	5.00	29.0	-29.9	-30.7	-31.1	179.9	5.16	28.8	**-29.0**	**-32.0**	**-32.6**	
57.2	4.63	28.8	***-29.9***	***-30.5***	***-31.0***	181.9	6.14	28.7	-29.8	-30.5	-31.0	
58.9	4.60	28.8	-29.7	-30.4	-31.0	184.0	5.41	28.7	-29.5	-30.4	-31.2	
60.6	4.66	28.8	-29.4	-30.9	-31.4	187.7	5.84	28.8	***-29.1***	***-32.0***	***-32.6***	
62.5	4.81	28.9	-29.9	-30.8	-32.4	191.9	6.44	28.7	-29.1	-30.9	-32.4	
65.5	4.12	28.8	**-29.8**	**-30.8**	**-32.3**	196.8	5.38	28.9	**-29.9**	**-30.7**	**-32.1**	
68.5	4.68	28.7	-30.0	-31.1	-32.2	200.6	5.49	28.9	-29.6	-31.1	-31.7	
71.5	4.50	28.8	-30.7	-31.5	-32.2	205.8	5.80	28.8	-29.9	-30.6	-32.0	
74.1	4.45	28.8	**-29.7**	**-31.1**	**-32.4**	210.0	5.45	28.9	-29.4	-30.3	-31.1	
76.8	4.74	28.7	-29.9	-31.3	-32.3	212.6	4.60	29.2	**-29.9**	**-32.6**	**-30.8**	
79.4	4.78	28.8	-29.7	-30.8	-31.7	215.1	4.62	28.9	-30.1	-33.8	-31.5	
82.3	4.94	28.7	-29.7	-30.8	-31.1	217.8	4.52	28.9	-29.8	-33.1	-31.0	
85.6	6.13	28.8	***-29.5***	***-30.2***	***-31.3***	222.0	5.24	29.1	-29.9	-31.4	-31.6	
88.9	6.28	28.8	-30.1	-30.6	-31.3	225.1	4.71	28.9	-29.5	-31.0	-31.4	
92.2	6.30	28.7	-29.0	-29.9	-30.8	227.4	5.37	28.6	-30.0	-30.8	-30.9	
95.5	5.99	28.7	-29.4	-30.4	-31.1	229.8	5.90	28.8	***-29.3***	***-30.0***	***-31.3***	
98.8	6.14	28.8	**-29.2**	**-30.2**	**-30.6**	232.1	4.62	28.9	-28.4	-30.3	-31.0	
102.1	5.22	28.6	-29.6	-29.8	-30.5	235.3	4.09	29.0	-30.9	-32.2	-31.6	
105.4	5.63	28.7	-29.3	-30.0	-30.5	239.9	2.90	29.0	-30.4	-33.3	-32.3	
111.2	5.06	28.7	-29.5	-30.2	-30.9	244.5	2.87	29.0	-30.8	-31.6	-33.1	
118.7	5.36	28.9	-30.0	-30.8	-31.3	249.1	3.68	29.0	-31.0	-32.1	-33.8	
127.1	5.48	28.9	-29.5	-30.5	-31.2	257.3	2.91	29.0	**-30.8**	**-31.6**	**-33.0**	
135.3	4.91	28.9	**-29.9**	**-30.8**	**-30.6**	257.4	3.56	29.0	-31.5	-32.5	-33.8	
139.3	4.77	29.0	-30.4	-31.2	-32.3	261.1	3.64	29.0	-31.0	-32.3	-33.9	
143.3	4.85	29.0	***-30.2***	***-30.7***	***-31.5***	264.2	3.55	29.1	-30.2	-30.3	-33.8	
147.2	5.17	29.0	-30.0	-30.5	-31.7	267.3	3.30	29.0	-30.9	-31.9	-33.9	

Bold $\delta^{13}C$ values are duplicates while bold-italic values are triplicates.

FIGURE CAPTIONS

Fig. 1 Locations of piston cores from the North Pacific Ocean (ES) and the Bering Sea (BOW-8a), Cruise KH99-3 and Site 883, ODP Leg 145.

Fig. 2 Magnetic susceptibilities and benthic foraminifera oxygen isotopes from the North Pacific Ocean (ES) core and Site 883, oxygen isotope from the Bering Sea (BOW-8a) core, and SPECMAP stack curve plotted against age in ka.

Fig. 3 Representative total ion chromatograms of *n*-alkanes from the ES (0.80–0.85 mbsf) and BOW-8a (0.70-0.75 mbsf). Predominance of long chain *n*-alkane (C_{27}, C_{29}, or C_{31}) can be seen throughout both cores.

Fig. 4 Vertical distribution of oxygen isotope, $\delta^{13}C$ values of land plant derived *n*-alkanes (C_{27}, C_{29}, and C_{31}), average chain lengths (ACL), carbon preference index (CPI) and mass accumulation rates of long chain *n*-alkanes ($C_{27}+C_{29}+C_{31}$) from the North Pacific Ocean (ES) core.

$$CPI=0.5x[(C_{25}+C_{27}+C_{29}+C_{31}+C_{33})/(C_{24}+C_{26}+C_{28}+C_{30}+C_{32})+ (C_{25}+C_{27}+C_{29}+C_{31}+C_{33})/(C_{26}+C_{28}+C_{30}+C_{32}+C_{34})]$$

$$ACL= [27(C_{27})+29(C_{29})+31(C_{31})]/ (C_{27}+C_{29}+C_{31})$$

Fig. 5 Vertical distribution of oxygen isotope, $\delta^{13}C$ values of land plant derived *n*-alkanes (C_{27}, C_{29}, and C_{31}), average chain lengths (ACL), carbon preference index (CPI) and mass accumulation rates of long chain *n*-alkanes ($C_{27}+C_{29}+C_{31}$) from the Bering Sea (BOW-8a) core.

$$CPI=0.5x[(C_{25}+C_{27}+C_{29}+C_{31}+C_{33})/(C_{24}+C_{26}+C_{28}+C_{30}+C_{32})+ (C_{25}+C_{27}+C_{29}+C_{31}+C_{33})/(C_{26}+C_{28}+C_{30}+C_{32}+C_{34})]$$

$$ACL=[27(C_{27})+29(C_{29})+31(C_{31})]/ (C_{27}+C_{29}+C_{31})$$

Fig. 6 The $\delta^{13}C$ of *n*-C_{29} alkane versus average chain length (ACL) of *n*-C_{27}, *n*-C_{29}, and *n*-C_{31} alkanes from the North Pacific Ocean (ES) core, and the Bering Sea (BOW-8a) core.

Fig. 1

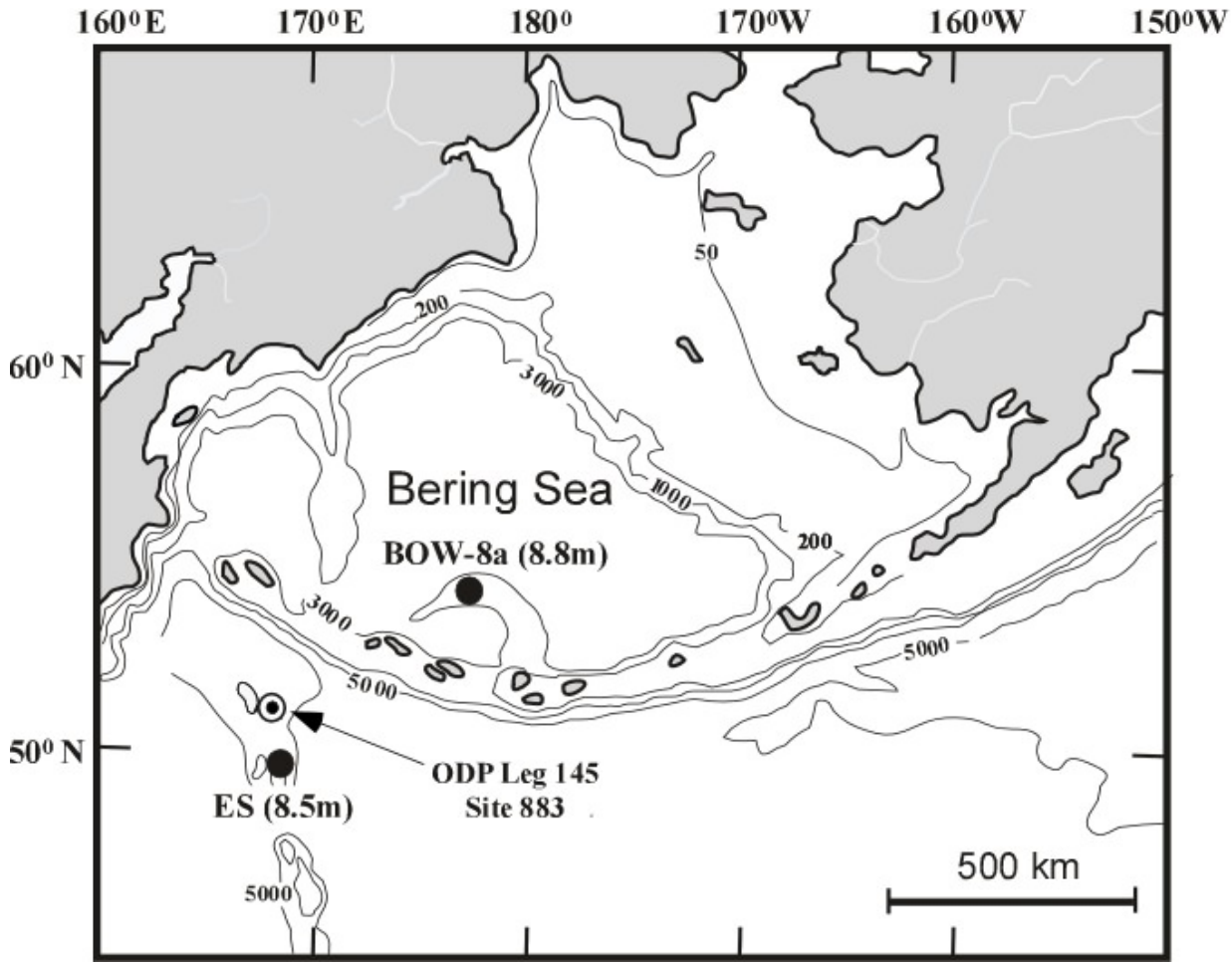
160⁰ E
170⁰ E
180⁰
170⁰W
160⁰W
150⁰W
60⁰ N
50⁰ N
50
200
3000
Bering Sea
1000
BOW-8a (8.8m)
200
3000
5000
5000
ODP Leg 145
Site 883
ES (8.5m)
5000
500 km

Fig. 2

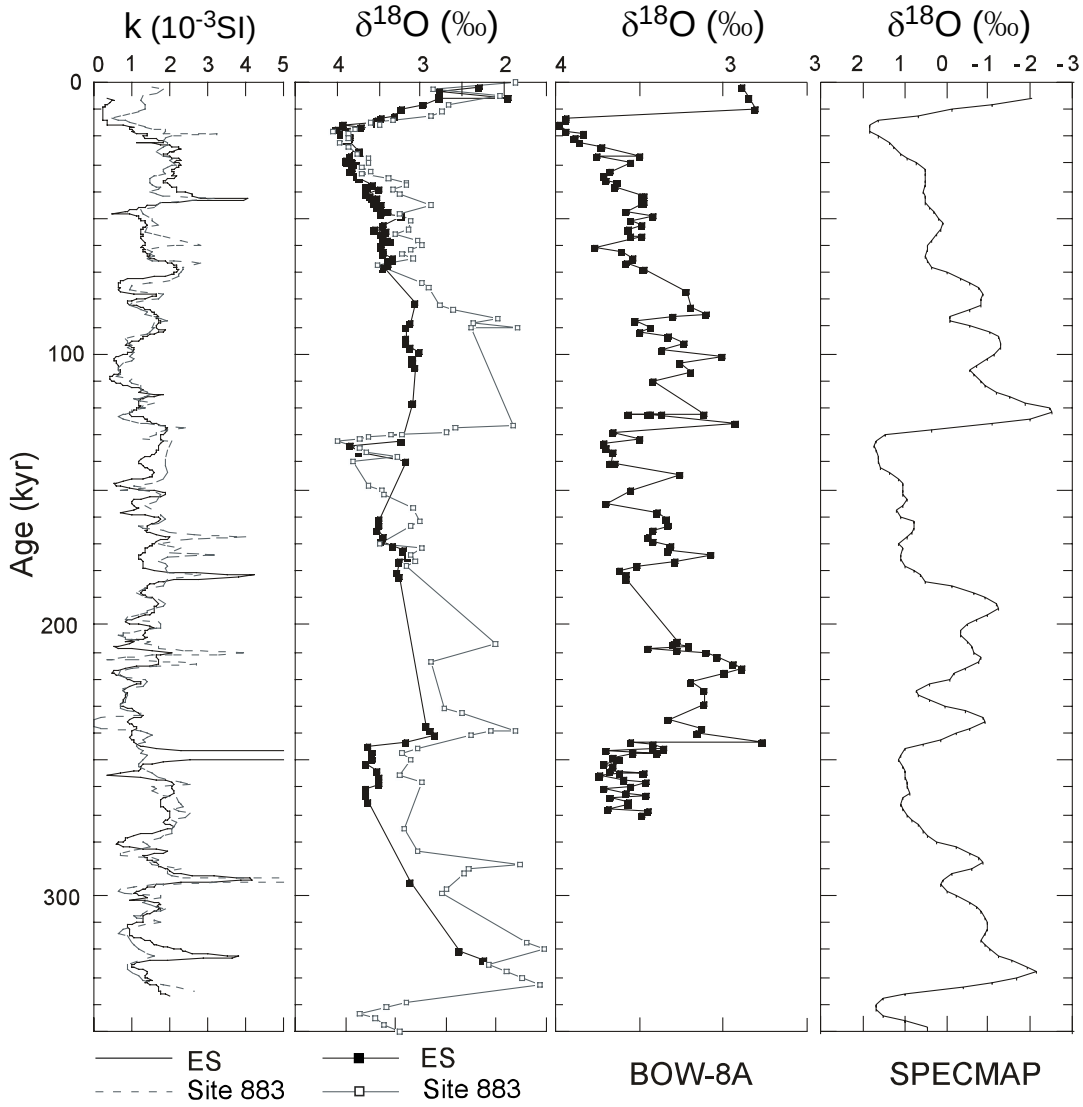
k (10-3SI)
δ18O (‰)
δ18O (‰)
δ18O (‰)
0 1 2 3 4 5
4 3 2
4 3
3 2 1 0 -1 -2 -3
0
100
200
300
Age (kyr)
ES
Site 883
ES
Site 883
BOW-8A
SPECMAP

Fig. 3

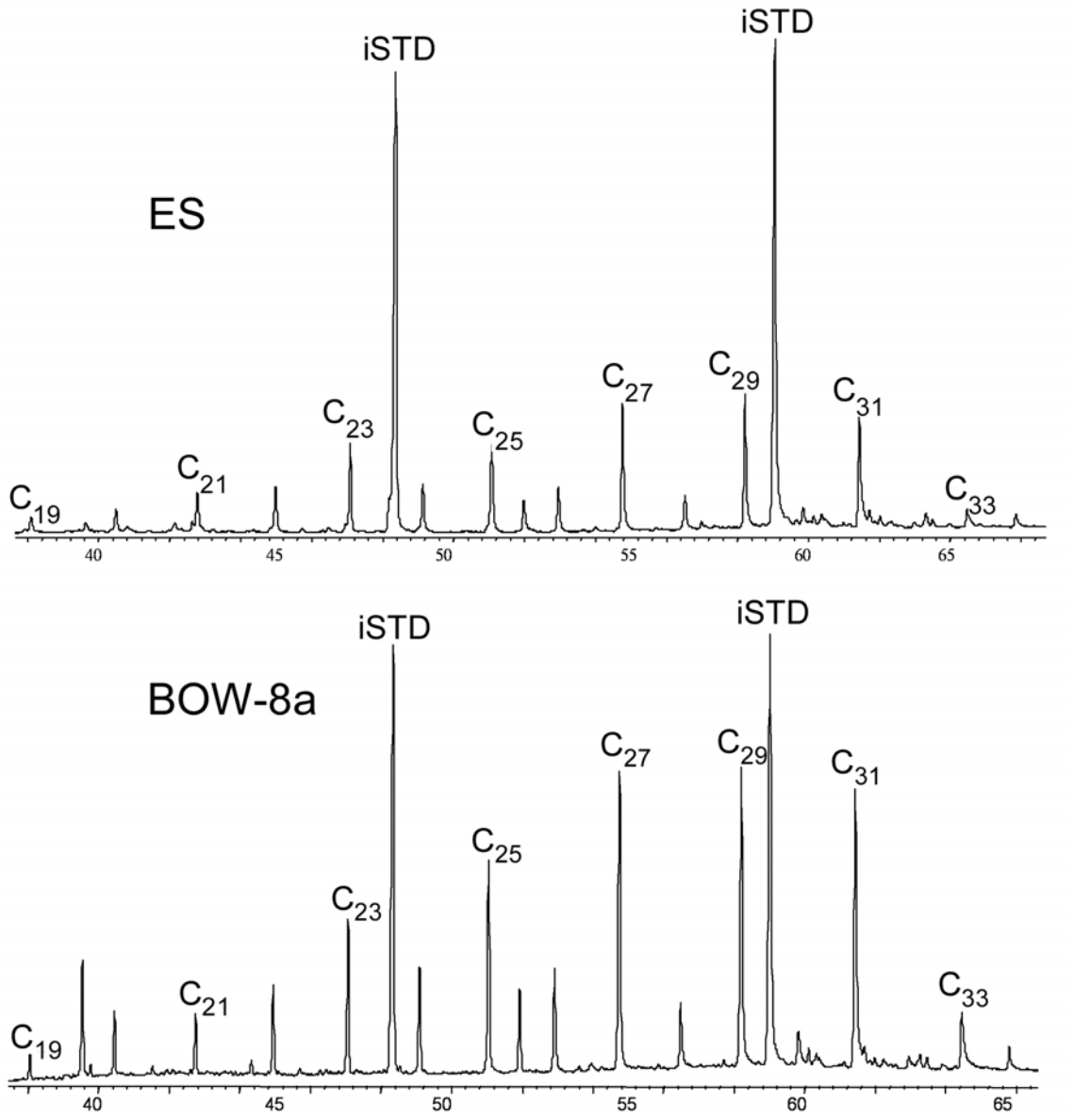
ES
iSTD
iSTD
C19
C21
C23
C25
C27
C29
C31
C33
40
45
50
55
60
65
BOW-8a
iSTD
iSTD
C19
C21
C23
C25
C27
C29
C31
C33
40
45
50
55
60
65

Fig. 4

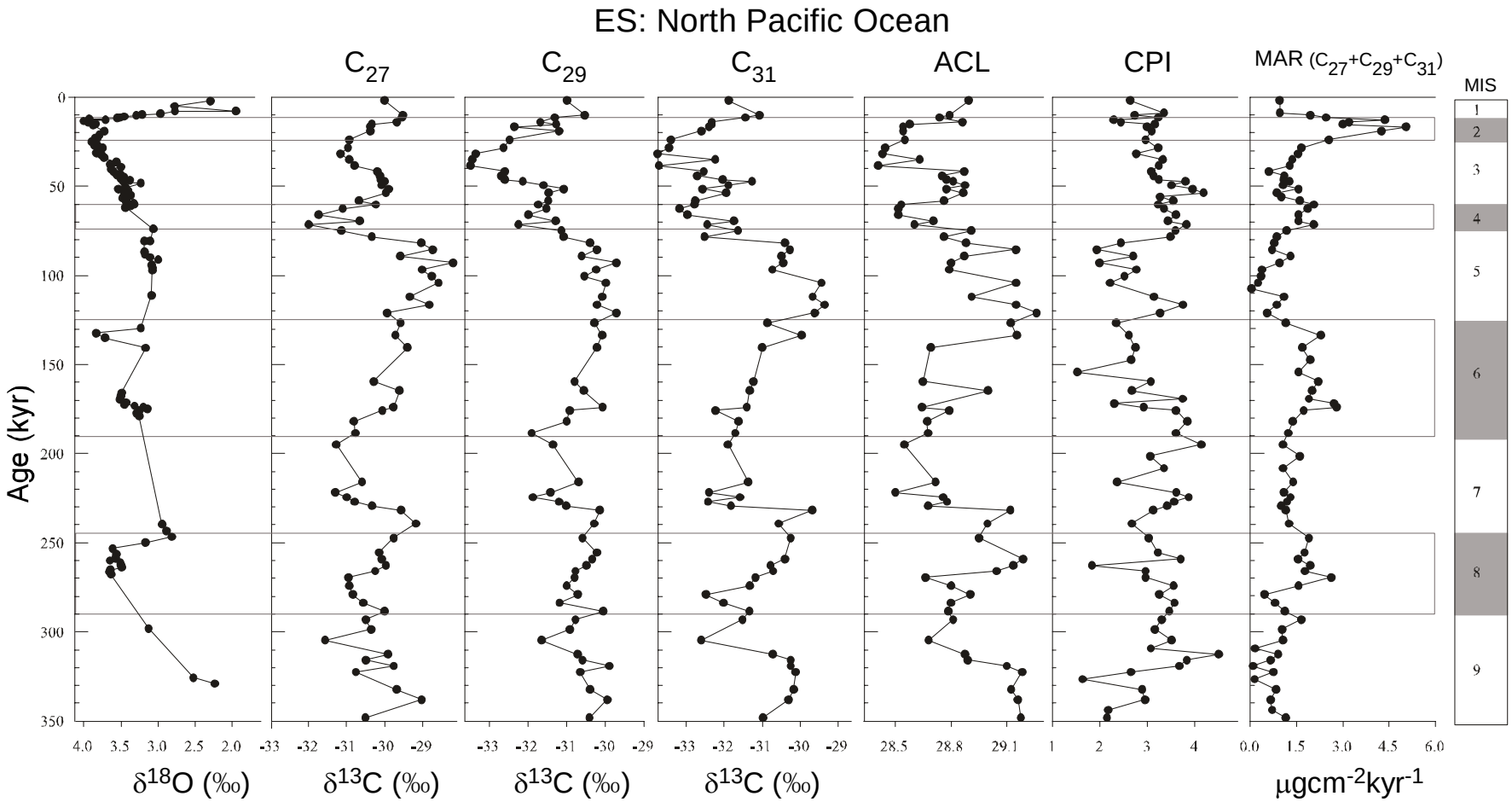
ES: North Pacific Ocean
C27
C29
C31
ACL
CPI
MAR (C27+C29+C31)
MIS
Age (kyr)
δ18O (‰)
δ13C (‰)
δ13C (‰)
δ13C (‰)
μgcm-2kyr-1

Fig. 5

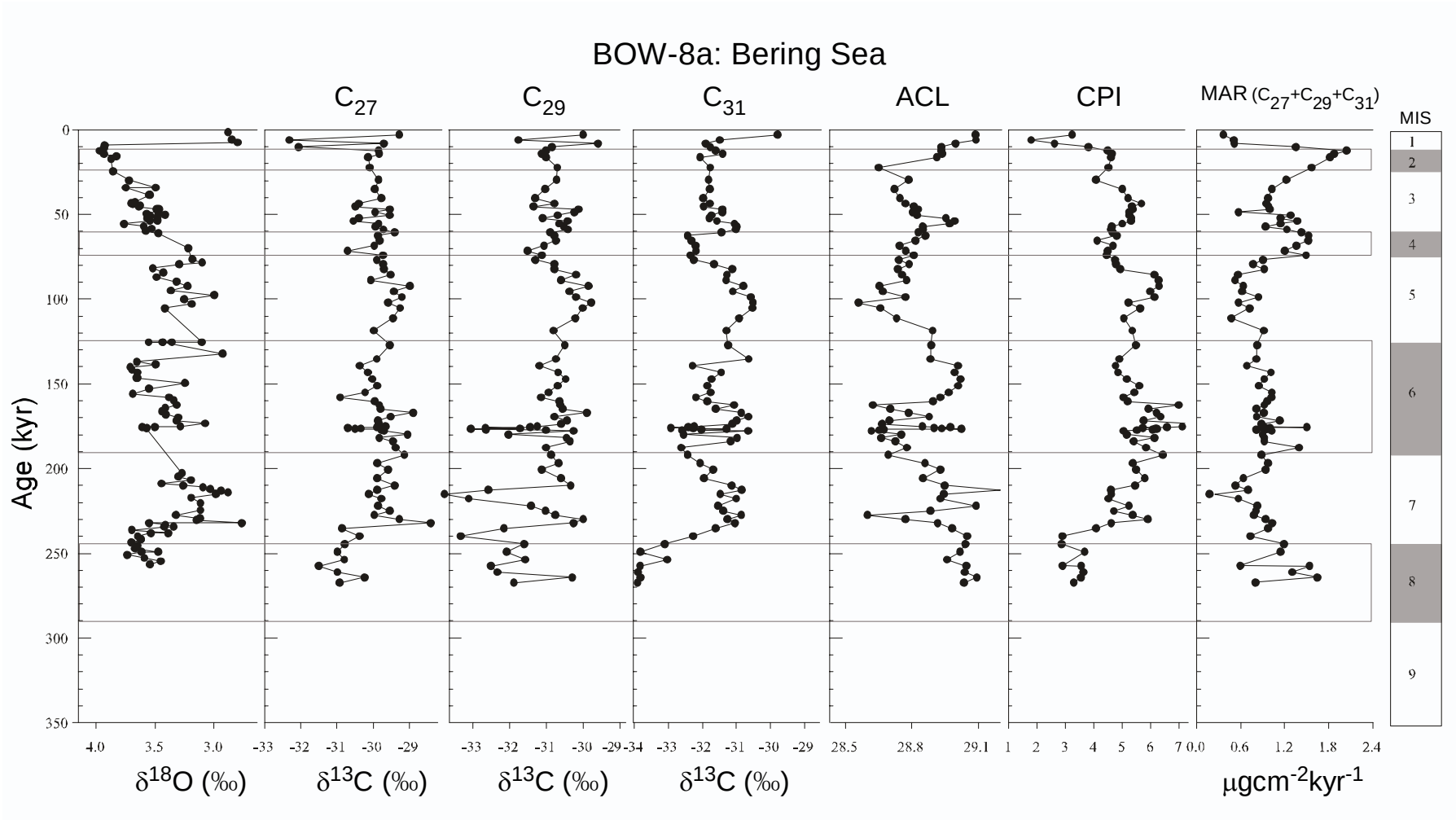
BOW-8a: Bering Sea
C27
C29
C31
ACL
CPI
MAR (C27+C29+C31)
MIS
Age (kyr)
0
50
100
150
200
250
300
350
1
2
3
4
5
6
7
8
9
4.0
3.5
3.0
δ18O (‰)
-33
-32
-31
-30
-29
δ13C (‰)
-33
-32
-31
-30
-29
δ13C (‰)
-34
-33
-32
-31
-30
-29
δ13C (‰)
28.5
28.8
29.1
1
2
3
4
5
6
7
0.0
0.6
1.2
1.8
2.4
μgcm-2kyr-1

Fig. 6

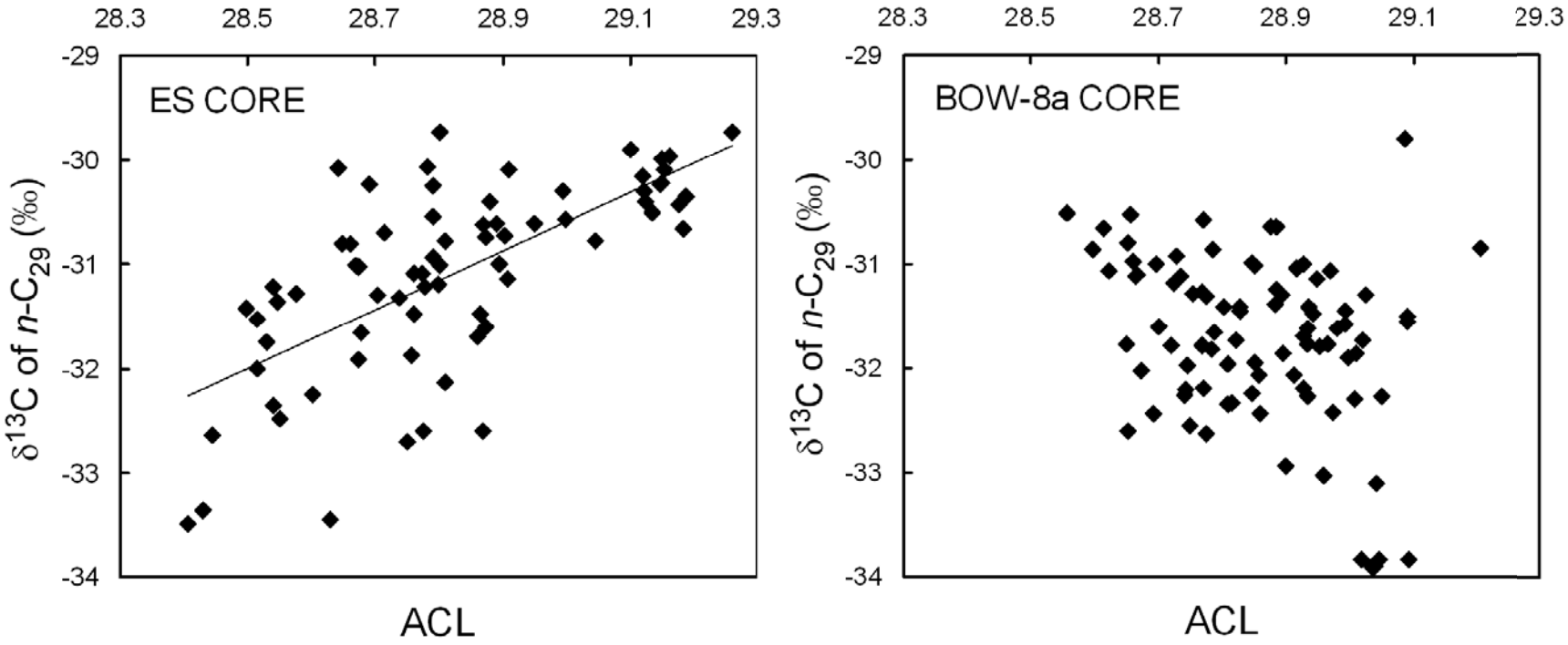
ES CORE
BOW-8a CORE
28.3
28.5
28.7
28.9
29.1
29.3
-29
-30
-31
-32
-33
-34
δ13C of n-C29 (‰)
ACL